Electronic Supplementary Material (ESI) for Journal of Materials Chemistry A.

Supporting Information

Nitrogen-doped CoP nanoarray over 3D porous Co foam as efficient bifunctional electrocatalysts for overall water splitting

Zong Liu, Xu Yu, Huaiguo Xue and Ligang Feng[*]

School of Chemistry and Chemical Engineering, Yangzhou University, Yangzhou 225002, China

[*]Corresponding authors.

E-mail addresses: ligang.feng@yzu.edu.cn, fenglg11@gmail.com (L. Feng).

Experimental Section

Synthesis of cobalt carbonate hydroxide hydrate precursor. 0.44g of $Co(NO_3)_2 \cdot 6H_2O$, 0.14 g of NH_4F and 0.45 g of urea was dissolved in a 30 mL deionized water under vigorous stirring for 10 min; then, the mixed solution was transferred into the autoclave and cobalt foam with the size of 2 cm×2 cm was immersed in the reactor. The autoclave was treated under 120 °C for 6 h. The Co foam were cleaned by hydrochloric acid, ethanol and distilled water, respectively, before use. After cooling down to room temperature, the pink precipitate was found coated over the Co foam and finally, cobalt carbonate hydroxide hydrate precursor containing N element from the urea was obtained by drying at 60°C for 8 h under vacuum atmosphere. Similar approach has been employed to obtain the N-doped catalyst material reported elsewhere in the hydrothermal approach to introduce the N element.[1-3]

Synthesis of CoP-N/Co foam. CoP-N/Co foam was synthesized by the thermal annealing of cobalt carbonate hydroxide hydrate precursor containing N element and NaH_2PO_2 in a tube furnace. The mass ratio of cobalt carbonate hydroxide hydrate to NaH_2PO_2 is 1:2 was placed in a corundum crucible. The NaH_2PO_2 was put at the upstream and cobalt carbonate hydroxide hydrate precursor was placed at the downstream side. The thermal decomposition process was heated to 300 ˚C at a ramping rate of 3 ˚C min^{-1} and maintained for 4 h under nitrogen flow protection. Finally, the obtained CoP-N/Co foam was washed by water and ethanol, and then dried at 60 ˚C for 12 h under vacuum. The mass loading of the N doped CoP on Co foam was calculated by measuring the weight difference between the initial Co foam and N doped CoP coated Co foam.

Synthesis of CoP /Co foam. In order to remove impurity elements (N) from the cobalt carbonate hydroxide hydrate precursor, the cobalt carbonate hydroxide hydrate precursor was transferred to Co_3O_4 by thermal annealing at 350 ˚C for 2 h under air atmosphere (Figure S1). Then, the CoP/Co foam was synthesized by the thermal decomposition of purified precursor and NaH_2PO_2 with a mass ratio of 1:2. They were put in to a corundum crucible at the upstream and downstream side, and then put into a tube furnace. The thermal decomposition process was at a ramping rate of 3 ˚C min^{-1} heat to 300 ˚C maintained for 4 h under nitrogen flow protect. Finally, the obtained CoP

/Co foam was washed by water and ethanol, and then dried at 60 ˚C for 12 h under vacuum. The mass loading of the CoP on Co foam was calculated by measuring the weight difference between the initial Co foam and CoP coated Co foam.

Synthesis of P doped Co foam. The Co foam were cleaned by hydrochloric acid, ethanol and distilled water, respectively. And then the Co foam was dried at 50 ˚C for 8 h. The P doped Co foam was synthesized by the thermal decomposition of Co foam and NaH_2PO_2. In a mass ratio (Co foam/NaH_2PO_2) of 1:2, the NaH_2PO_2 and Co foam respectively was put in corundum crucible at the upstream and downstream side, and then put into a tube furnace. The thermal decomposition process was at a ramping rate of 3 ˚C min^{-1} heat to 300 ˚C maintained for 4 h under nitrogen flow protect. Finally, the obtained P doped Co foam was washed by water and ethanol, and then dried at 60 ˚C for 12 h under vacuum. The mass loading of the P doped Co foam was calculated from the weight difference between the initial Co foam and P doped Co foam.

Characterization

Powder X-ray diffraction (XRD) patterns were recorded on a Bruker D8 Advance Powder X-ray diffractometer using a Cu Kα (λ = 1.5405 Å) radiation source operating at 40 kV and 40 mA, and at a scanning rate of 5 ° min^{-1}. A fine powder sample was ground, then put on the glass slide and pressed to make a flat surface under the glass slide. All transmission electron microscopy (TEM) and high-resolution TEM (HRTEM) measurements were conducted on a TECNAI G2 operating at 200 kV. The element mapping analysis and energy dispersive X-ray detector spectrum (EDX) images were obtained on a TECNAI G2 transmission electron microscope equipped with an EDXA detector: the microscope was operated at an acceleration voltage of 200 kV. All X-Ray photoelectron spectroscopy (XPS) measurements were carried out on a Kratos XSAM-800 spectrometer with an Al Kα radiation source. The mass content of the catalyst was measured by a precise balance with the accuracy of 1/100 000g (Sartorius Quintix®, quintix35-1CN)

All the electrochemical measurements were performed with a Bio-Logic VSP electrochemical workstation (Bio-Logic Co., France). The OER and HER performance was measured in a three-electrode electrochemical cell. A saturated calomel electrode (SCE, Hg/Hg_2Cl_2) electrode was used as the reference electrode through a double salt-

bridge and luggin capillary tip, and it was carefully calibrated before and after the measurement to ensure the accuracy. A graphite rod was used as the counter electrode. Potentials were referenced to a reversible hydrogen electrode (RHE) by adding a value of (0.24 + 0.0592*pH) V. All potentials were converted and referred to the RHE unless stated otherwise. A sample (1 cm×0.5 cm foam) was used as the working electrode. A total electrolyte volume of ~50 mL was used to fill the glass cell. The cyclic voltammetry experiments for the OER and HER were conducted in 1 M KOH at 25 °C using a working electrode and a scan rate of 5 mV s^{-1}. The preparation of the Pt/C/Co foam and RuO_2/Co foam samples was shown in detail as follows: 5 mg of Pt/C or RuO_2 catalysts, 960 μL ethanol and 40 μL Nafion solution were mixed, and then sonicated for 30 min to make a homogeneous dispersion. 50 μL of the catalysts ink was loaded onto the Co foam (1 cm×0.5 cm) by drop casting as the working electrode with a mass loading of 0.25 mg cm^{-2}. Prior to recording the OER and HER activity of as-preparation catalysts, the catalysts were activated by 50 cyclic voltammetry scans in 1 M KOH at a scan rate of 20 mV s^{-1}.

The electrochemical surface area (ECSA) was evaluated in terms of doubler layer capacitance (C_{dl}). The ECSA was estimated by cyclic voltammetry (CV) without Faradaic processes occurred region from 0.025 to 0.225 V in 1 M KOH at scan rate 20, 40, 60, 80 and 100 mV s^{-1}. The C_{dl} was estimated by plotting the $\triangle J = (J_a - J_c)/2$ at 0.125 V vs. RHE against the scan rate. The linear slope is the double layer capacitance $C_{dl.}$ The specific capacitance is evaluated for a flat surface by assuming 40 μF cm^{-2} according to previous literature.[4-7] The electrochemically active surface area was achieved by normalizing the doubler layer capacitance to a standard specific capacitance.

Turnover frequency (TOF) was calculated using the following equation (lower TOF limits were calculated) [8, 9]:

$$\text{OER: TOF} = \frac{J \times A}{(4 \times F \times n)}$$

$$\text{HER: TOF} = \frac{J \times A}{(2 \times F \times n)}$$

J is the current density at a specific overpotential (A cm^{-2}). *A* is the geometric area of the Co foam-based samples. *F* is the faraday constant (96485 mol C^{-1}). *n* is the total number of moles of all the active metal sites (Co metal ions) that were deposited onto the Co foam. The moles of metal ions were calculated based on the equation: *(D*A)/M*,

D is the loading density, *M* is the relative molecular mass.

A gas-tight electrochemical cell coupling with a gas burette was carried out to verify the faradaic yield of samples. The working electrode was prepared by drop-casting catalyst suspension on the Co foam with the surface area of 1 cm^{-2}. A constant overpotential (-100 mV vs. RHE and 1.49 V vs. RHE) was applied on the electrode and the volume of the evolved gas was recorded synchronously. Thus, the faradaic yield was calculated from the ratio of the recorded gas volume to the theoretical gas volume during the charge passed through the electrode[10] (Figure S11):

$$Faradaic\ yield = \frac{V_{experimental}}{V_{theoretical}} = \frac{V_{experimental}}{\frac{1(2)}{4} \times \frac{Q}{F} \times V_m}$$

where Q is the charge passed through the electrode, F is Faraday constant (96485 C mol^{-1}), the number 4 means 4 mole electrons per mole O_2, the number 1 (2) means 1 O_2 (2 mole H_2) mole, V_m is molar volume of gas (24.5 L mol^{-1}, 298 K, 101 KPa).

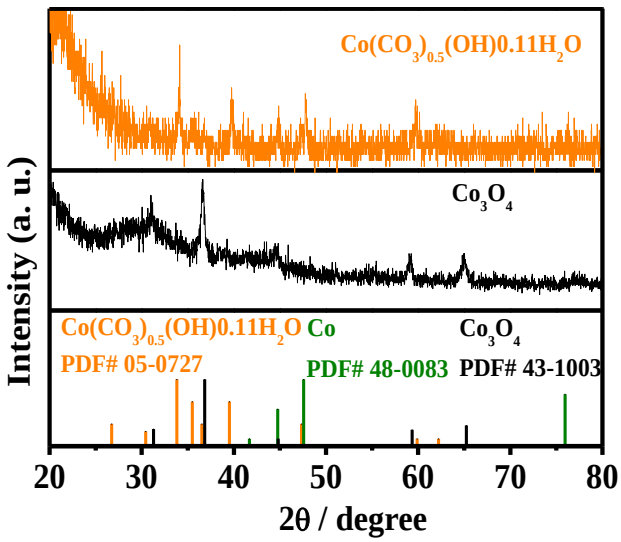

Figure S1. XRD patterns of cobalt carbonate hydroxide hydrate precursor and after purified precursor.

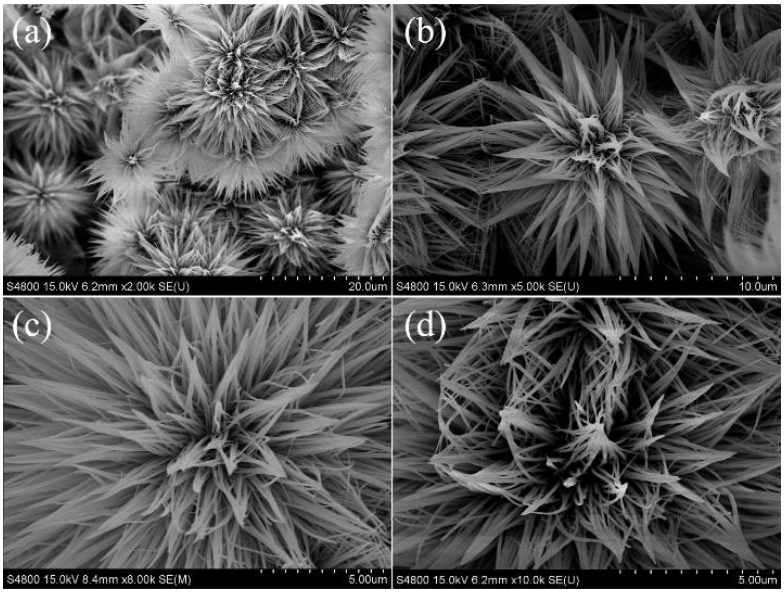

Figure S2a. SEM images of cobalt carbonate hydroxide hydrate precursor.

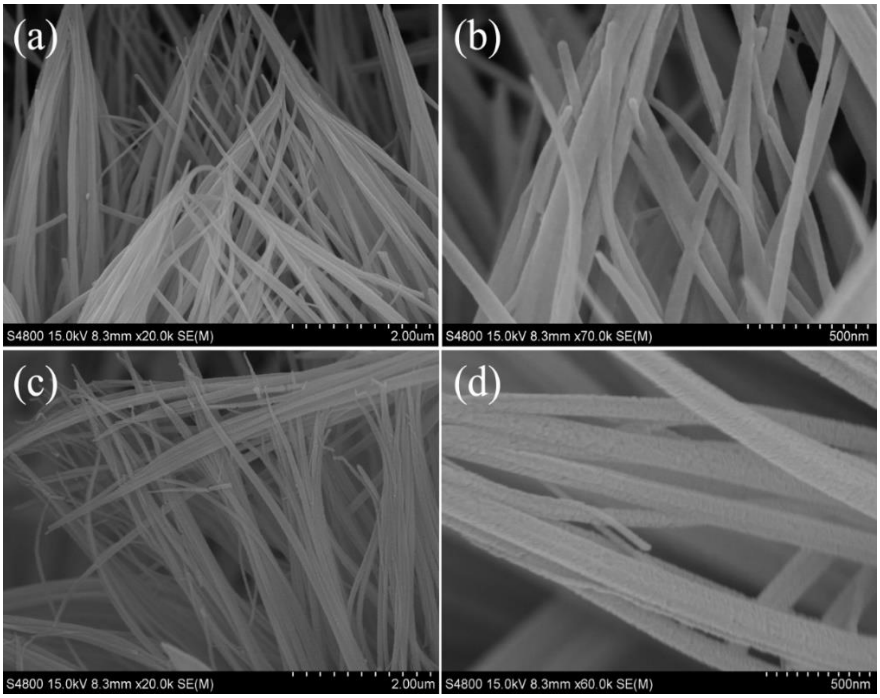

Figure S2b. SEM images of (a-b) cobalt carbonate hydroxide hydrate precursor and (c-d) CoP-N/Co foam.

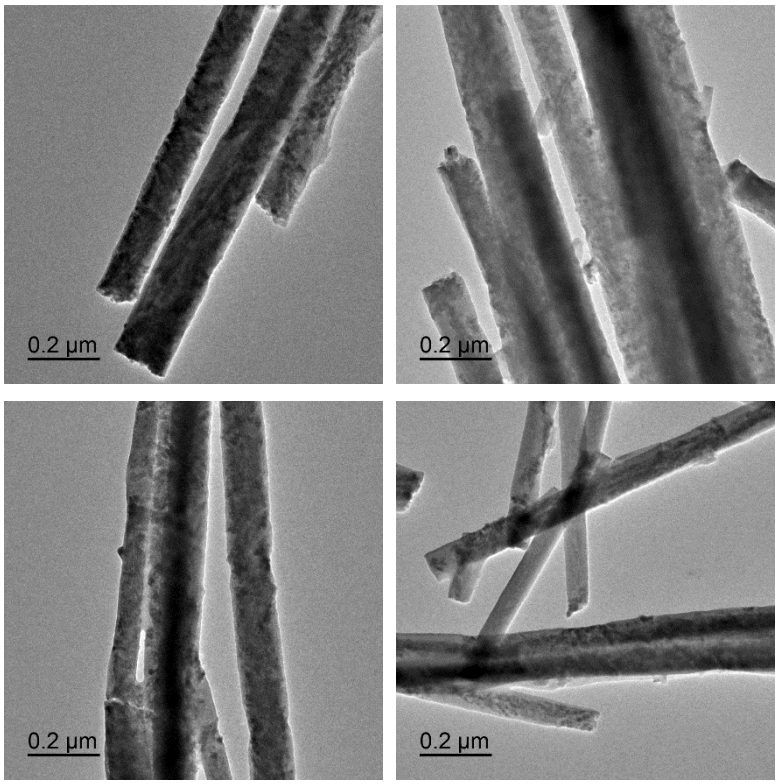

Figure S3. TEM images of CoP-N/Co foam.

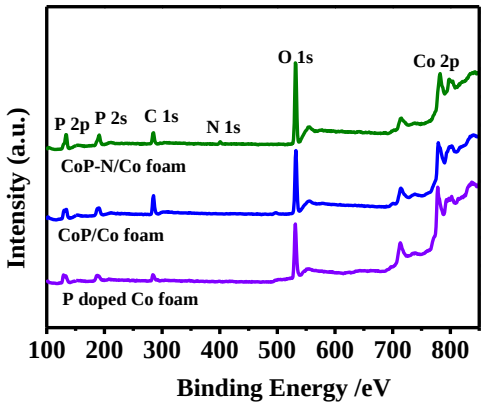

Figure S4. XPS survey scan of CoP-N/Co foam, CoP/Co foam and P doped Co foam.

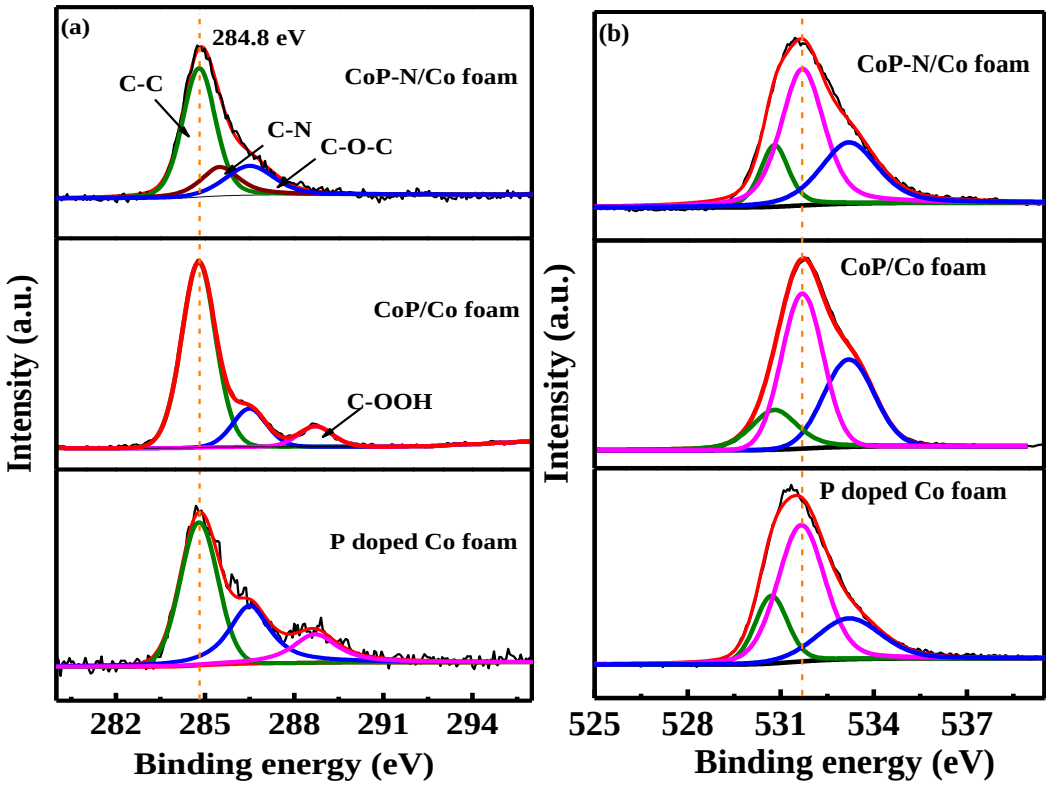

Figure S5. XPS spectra of (a) C 1s, and (b) O 1s of CoP-N/Co foam, CoP/Co foam and P doped Co foam.

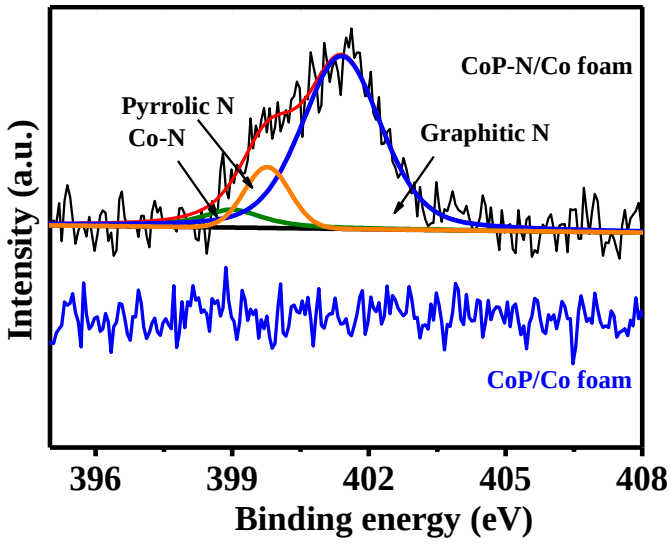

Figure S6. XPS spectra of N 1s of CoP-N/Co foam and CoP/Co foam.

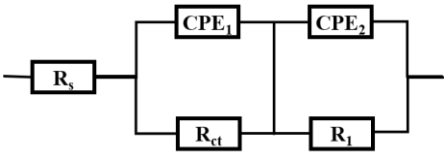

Figure S7. The equivalent circuit model of EIS analysis of all samples.

The equivalent circuit includes a parallel combination of (R_1, CPE_2) and (R_{ct}, CPE_1) element in series with R_s. The CPE generally was employed to well fit the impedance data by safely treating as an empirical constant without considering the its physical basis. And mostly, it was regarded as the double layer capacitor from the catalyst/support and catalyst solution. R_s was a sign of the uncompensated solution resistance, R_{ct} was a charge transfer resistance arisen from the relevant electro-chemical oxidation, R_1 was associated to the contact resistance between the catalyst material and the others resistance.

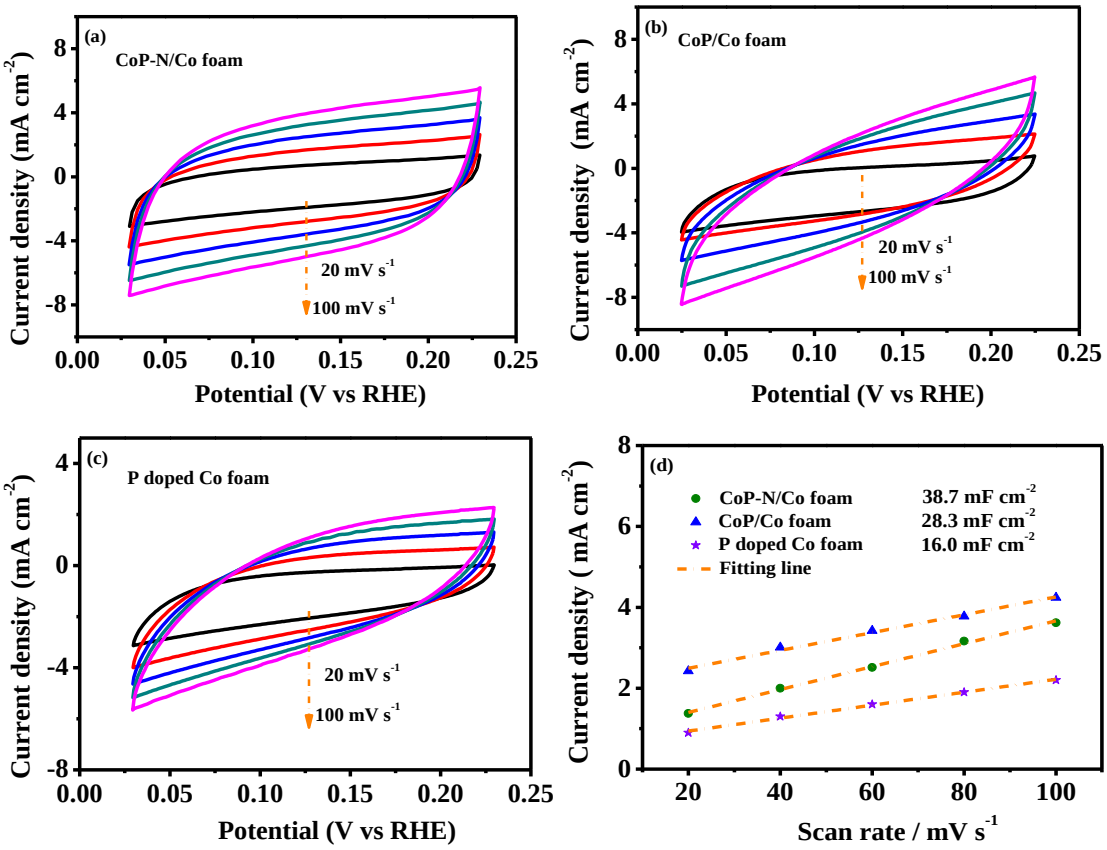

Figure S8. (a)-(c) Cyclic voltammograms of CoP-N/Co foam, CoP/Co foam and P doped Co foam in the non-faradaic capacitance from 0.025 V to 0.225 V vs. RHE current range at scan rates of 20, 40, 60, 80 and 100 mV/s. (d) Calculated electrochemical double-layer capacitance for CoP-N/Co foam, CoP/Co foam and P doped Co foam.

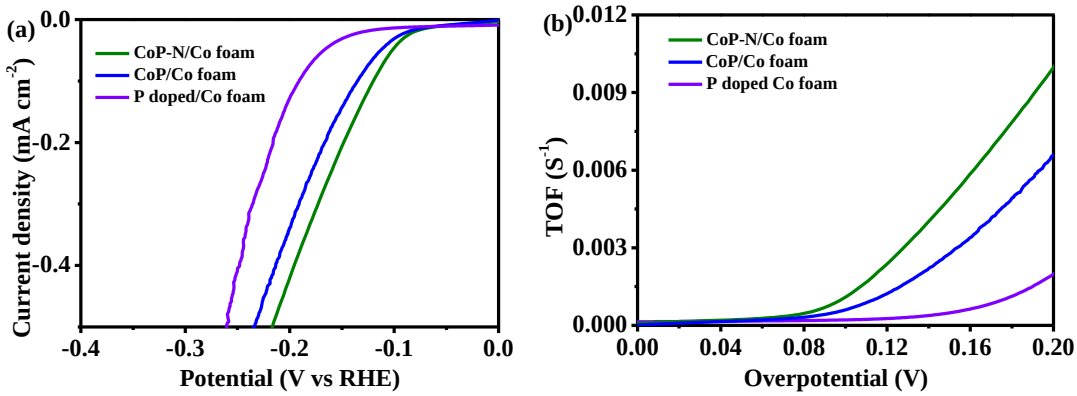

Figure S9. (a) Specific HER activity of as-prepared catalysts. Polarization curves are normalized by the electrochemical active surface areas, which indicates the higher specific activity of the CoP-N/Co foam than the HER activities of CoP/Co foam and P doped Co foam. (b) TOF values of the as-prepared catalysts as a function of overpotential.

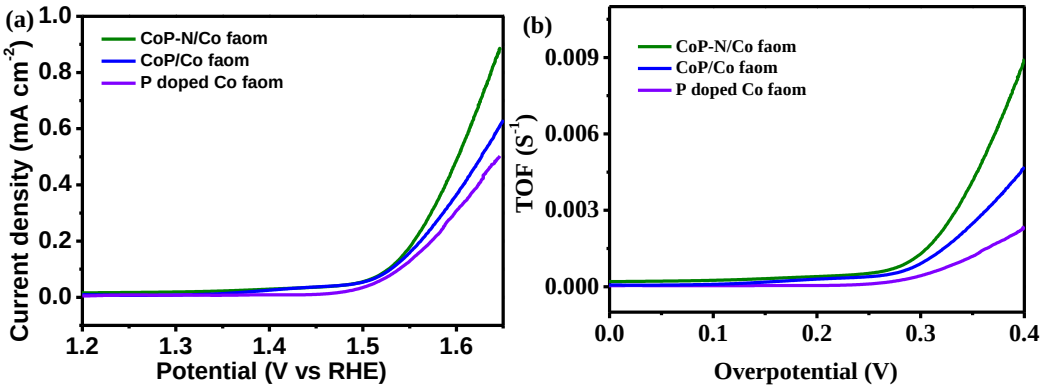

Figure S10. (a) Specific OER activity of as-prepared catalysts. Polarization curves are normalized by the electrochemical active surface areas, which indicates the higher specific activity of the CoP-N/Co foam than the OER activities of CoP/Co foam and P doped Co foam. (b) TOF values of the as-prepared catalysts as a function of overpotential.

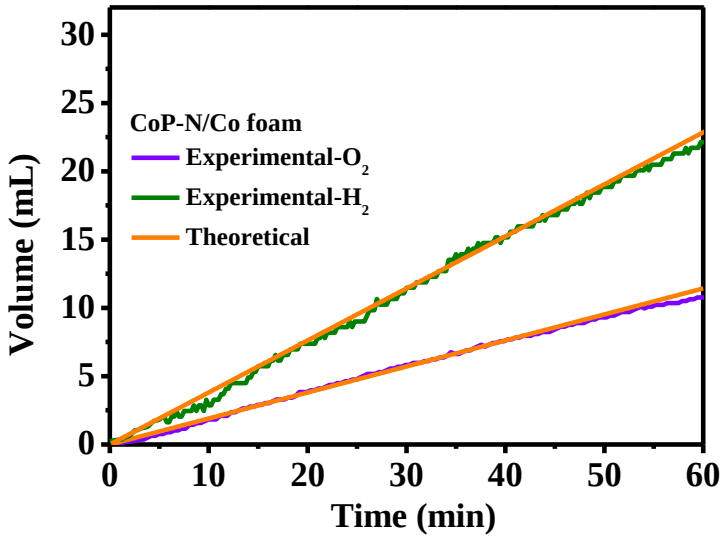

Figure S11. The tested volume of O_2 and H_2 gas released versus water splitting time with the CoP-N/Co foam. (At 50 mA cm^{-2} in 1 M KOH.)

The theoretical line represents the expected amounts of H_2 and O_2 assuming a quantitative of 100% Faradaic yield. The Faradaic yield is closing to 100%, which were calculated under charge passed through the electrode by the ratio of the observed gas volume to the theoretical gas volume calculated. The loss may be attributing to the attached bubbles on working electrode surface and the dissolved gas in the KOH solution.

Table S1. XPS spectrum fitting for peak position of samples.

Samples	Co 2p3/2		Co 2p1/2	
CoP-N/Co foam	778.4	781.6	793.4	797.5
CoP /Co foam	778.4	781.6	793.4	797.5
P doped Co foam	778.1	781.0	793.1	796.9

Table S2. Comparison of HER and OER performance in 1 M KOH for reported transition metal catalysts.

Materials	Mass loading (mg/cm^2)	Electrode substrate	Overpotential (vs. RHE)		Reference
			HER	OER	
CoP-N/Co foam	1.9	Co foam	60(100) ($\eta_{10}(\eta_{50})$)	260(η_{50})	This work
RuO_2/Co Foam	0.25	Co foam	-	322 (η_{50})	This work
Pt/C/Co Foam	0.25	Co foam	40(77) ($\eta_{10}(\eta_{50})$)	-	This work
np-$(Ni_{0.67}Fe_{0.33})_4P_5$	-	Carbon fiber	120(η_{10})	275(η_{50})	[11]
$Ni_{0.51}Co_{0.49}P$-NF	-	Ni foam	82(η_{10})	280(η_{50})	[12]
Co_2P/Co-foil	-	Co foil	157(η_{10})	319(η_{10})	[13]
$Co_{0.93}Ni_{0.07}P_3$ /CC	1.05	Carbon cloth	87(η_{10})	330(η_{50})	[14]
CoP NS/CC	0.28	Carbon cloth	90(η_{10})	310(η_{10})	[15]
$Ni_{1.5}Fe_{0.5}P$	1.38	Carbon fiber	282(η_{10})	264(η_{10})	[16]
CoP@NF	1.2	Ni foam	109(η_{10})	270(η_{10})	[17]
$Ni_{12}P_5$/NF	3	Ni foam	170(η_{10})	272(η_{20})	[18]
Co/CoP-5	0.88	Glass carbon	193(η_{10})	320(η_{20})	[19]
Co_2P	-	Glass carbon	75(η_{10})	320(η_{20})	[20]

Table S3. EIS fitting parameters from equivalent circuits of samples during HER process.

Samples	R_s / Ω cm^{-2}	R_1 / Ω cm^{-2}	CPE_1 / S s^{-n}	n /0<n<1	R_{ct} / Ω cm^{-2}	CPE / S s^{-n}	N /0<n<1
CoP-N/Co foam	3.45	2.06	1.334E-1	0.46	8.1	4.056E-2	0.83
CoP/Co foam	3.61	3.43	7.335E-2	0.96	26.1	9.013E-2	0.46
P doped Co foam	3.40	19.0	2.461E-3	0.81	320	2.199E-2	0.64

The resistance in the high frequency region revealed the resistance including electrolyte from the working electrode to the counter electrode, material itself and others resistance, which is independent of the applied potential.[21, 22] In the low-frequency region, the resistance is indicated by the mass transfer during electrocatalytic reactions corresponding to the electrocatalytic kinetics.[23]

Table S4 EIS fitting parameters from equivalent circuits of samples during OER process.

Samples	R_s / Ω cm^{-2}	R_1 / Ω cm^{-2}	CPE_1 / S s^{-n}	n / 0<n<1	R_{ct} / Ω cm^{-2}	CPE / S s^{-n}	n /0<n<1
CoP-N/Co foam	3.60	2.03	1.456E-1	0.48	9.0	9.802E-2	0.89
CoP/Co foam	3.53	3.91	1.753E-1	0.42	21.8	4.277E-1	0.88
P doped Co foam	3.48	5.31	2.402E-1	0.55	46.5	1.105E-1	0.95

Table S5. Summary of overall alkaline water splitting activity at 1 M KOH of recently reported bifunctional non-noble electrocatalysts.

Materials	Electrode substrate	Potential at 10 or 50 mA cm^{-2} (vs. RHE)	Reference
CoP-N/Co foam || CoP-N/Co foam	Co foam	1.49 (10) 1.61 (50)	This work
RuO_2/Co foam || Pt/C/Co foam	Co foam	1.51 (10) 1.78 (50)	This work
CoP/NF || Co_2P/ NF	Ni foam	1.61 (20)	[20]
NiCoP-NF || NiCoP-NF	Ni foam	1.58 (10)	[24]
$Ni_{0.51}Co_{0.49}P$-NF || $Ni_{0.51}Co_{0.49}P$-NF	Ni foam	1.57 (10)	[12]
S:CoP@NF || S:CoP@NF	Ni foam	1.617 (10)	[17]
NiCoP films || NiCoP films	Cu mesh	1.59 (10)	[25]
CoP NS/CC || CoP NS/CC	Carbon cloth	1.67 (10)	[15]
CoP/NCNHP || CoP/NCNHP	Glass carbon	1.64 (10)	[26]
Co_2P/Co-foil || Co_2P/Co-foil	Co foil	1.71 (10)	[13]
np-$(Ni_{0.67}Fe_{0.33})_4P_5$ || np-$(Ni_{0.67}Fe_{0.33})_4P_5$	Glass carbon	1.62 (10)	[11]
$Co_5Mo_{1.0}O$ NSs || $Co_5Mo_{1.0}P$ NSs	Ni foam	1.68 (10)	[27]
NiFe LDH@NiCoP/NF || NiFe LDH@NiCoP/NF	Ni foam	1.57 (10)	[28]
RuO_2/graphite paper||Pt–C/graphite paper	Graphite paper	1.53 (10) 1.85 (50)	[29]
RuO_2/CC||Pt–C/CC	Carbon cloth	1.60 (10) $_{about}$ 1.80 (50) $_{about}$	[30]
RuO_2||Pt–C	Ni foam	1.59 (10) $_{about}$ 1.83 (50) $_{about}$	[31]
Pt/C||RuO_2	Ni foam	1.54 (10)	[32]
RuO_2//Pt/C	Ni foam	1.54 (10)	[33]
RuO_2||Pt/C	Carbon fiber	1.57 (10) 1.80 (50) $_{about}$	[34]
RuO_2||Pt–C	Cobalt foam	1.56 (10)	[35]

References

[1] W. Zhang, Y. Sun, Q. Liu, J. Guo, X. Zhang, Vanadium and nitrogen co-doped CoP nanoleaf array as pH-universal electrocatalyst for efficient hydrogen evolution, Journal of Alloys and Compounds, 791 (2019) 1070-1078.

[2] Q. Wu, W. Li, D. Wang, S. Liu, Preparation and characterization of N-doped visible-light-responsive mesoporous TiO2 hollow spheres, Appl. Surf. Sci., 299 (2014) 35-40.

[3] H.-L. Guo, P. Su, X. Kang, S.-K. Ning, Synthesis and characterization of nitrogen-doped graphene hydrogels by hydrothermal route with urea as reducing-doping agents, J. Mater. Chem. A, 1 (2013) 2248-2255.

[4] C.C.L. McCrory, S. Jung, I.M. Ferrer, S.M. Chatman, J.C. Peters, T.F. Jaramillo, Benchmarking Hydrogen Evolving Reaction and Oxygen Evolving Reaction Electrocatalysts for Solar Water Splitting Devices, J. Am. Chem. Soc., 137 (2015) 4347-4357.

[5] C.C.L. McCrory, S. Jung, J.C. Peters, T.F. Jaramillo, Benchmarking Heterogeneous Electrocatalysts for the Oxygen Evolution Reaction, J. Am. Chem. Soc., 135 (2013) 16977-16987.

[6] Y. Ruquan, d.A.V. Paz, L. Yuanyue, A.J.M. Josefina, P. Zhiwei, W. Tuo, L. Yilun, Y.B. I., W. Su‐Huai, Y.M. Jose, T.J. M., High‐Performance Hydrogen Evolution from MoS2(1‒x)P x Solid Solution, Adv. Mater., 28 (2016) 1427-1432.

[7] G. Dingyi, Q. Jing, Z. Wei, C. Rui, Surface Electrochemical Modification of a Nickel Substrate to Prepare a NiFe‐based Electrode for Water Oxidation, ChemSusChem, 10 (2017) 394-400.

[8] L. Trotochaud, J.K. Ranney, K.N. Williams, S.W. Boettcher, Solution-Cast Metal Oxide Thin Film Electrocatalysts for Oxygen Evolution, J. Am. Chem. Soc., 134 (2012) 17253-17261.

[9] J. Jiang, A. Zhang, L. Li, L. Ai, Nickel–cobalt layered double hydroxide nanosheets as high-performance electrocatalyst for oxygen evolution reaction, J. Power Sources, 278 (2015) 445-451.

[10] W. Jun, L. Kai, Z. Hai‐xia, X. Dan, W. Zhong‐li, J. Zheng, W. Zhi‐jian, Z. Xin‐bo, Synergistic Effect between Metal‒Nitrogen‒Carbon Sheets and NiO Nanoparticles for Enhanced Electrochemical Water‐Oxidation Performance, Angew. Chem., Int. Ed., 54 (2015) 10530-10534.

[11] W. Xu, S. Zhu, Y. Liang, Z. Cui, X. Yang, A. Inoue, A nanoporous metal phosphide catalyst for bifunctional water splitting, J. Mater. Chem. A, 6 (2018) 5574-5579.

[12] J. Yu, Q. Li, Y. Li, C.-Y. Xu, L. Zhen, V.P. Dravid, J. Wu, Ternary Metal Phosphide with Triple-Layered Structure as a Low-Cost and Efficient Electrocatalyst for Bifunctional Water Splitting, Adv. Funct. Mater., 26 (2016) 7644-7651.

[13] C.-Z. Yuan, S.-L. Zhong, Y.-F. Jiang, Z.K. Yang, Z.-W. Zhao, S.-J. Zhao, N. Jiang, A.-W. Xu, Direct growth of cobalt-rich cobalt phosphide catalysts on cobalt foil: an efficient and self-supported bifunctional electrode for overall water splitting in alkaline media, J. Mater. Chem. A, 5 (2017) 10561-10566.

[14] Q. Fu, T. Wu, G. Fu, T. Gao, J. Han, T. Yao, Y. Zhang, W. Zhong, X. Wang, B. Song, Skutterudite-Type Ternary Co1–xNixP3 Nanoneedle Array Electrocatalysts for Enhanced Hydrogen and Oxygen Evolution, ACS Energy Lett., 3 (2018) 1744-1752.

[15] W. Zhu, W. Zhang, Y. Li, Z. Yue, M. Ren, Y. Zhang, N.M. Saleh, J. Wang, Energy-efficient 1.67 V single- and 0.90 V dual-electrolyte based overall water-electrolysis devices enabled by a ZIF-L derived acid–base bifunctional cobalt phosphide nanoarray, J. Mater. Chem. A, 6 (2018) 24277-24284.

[16] H. Huang, C. Yu, C. Zhao, X. Han, J. Yang, Z. Liu, S. Li, M. Zhang, J. Qiu, Iron-tuned super nickel

phosphide microstructures with high activity for electrochemical overall water splitting, Nano Energy, 34 (2017) 472-480.
[17] M.A.R. Anjum, M.S. Okyay, M. Kim, M.H. Lee, N. Park, J.S. Lee, Bifunctional sulfur-doped cobalt phosphide electrocatalyst outperforms all-noble-metal electrocatalysts in alkaline electrolyzer for overall water splitting, Nano Energy, 53 (2018) 286-295.
[18] P.W. Menezes, A. Indra, C. Das, C. Walter, C. Göbel, V. Gutkin, D. Schmeiβer, M. Driess, Uncovering the Nature of Active Species of Nickel Phosphide Catalysts in High-Performance Electrochemical Overall Water Splitting, ACS Catal., 7 (2017) 103-109.
[19] Z.-H. Xue, H. Su, Q.-Y. Yu, B. Zhang, H.-H. Wang, X.-H. Li, J.-S. Chen, Janus Co/CoP Nanoparticles as Efficient Mott–Schottky Electrocatalysts for Overall Water Splitting in Wide pH Range, Adv. Energy Mater., 7 (2017) 1602355.
[20] H. Li, Q. Li, P. Wen, T.B. Williams, S. Adhikari, C. Dun, C. Lu, D. Itanze, L. Jiang, D.L. Carroll, G.L. Donati, P.M. Lundin, Y. Qiu, S.M. Geyer, Colloidal Cobalt Phosphide Nanocrystals as Trifunctional Electrocatalysts for Overall Water Splitting Powered by a Zinc–Air Battery, Adv. Mater., 30 (2018) 1705796.
[21] H. Jin, S. Mao, G. Zhan, F. Xu, X. Bao, Y. Wang, Fe incorporated [small alpha]-Co(OH)2 nanosheets with remarkably improved activity towards the oxygen evolution reaction, J. Mater. Chem. A, 5 (2017) 1078-1084.
[22] W. Li, X. Gao, X. Wang, D. Xiong, P.-P. Huang, W.-G. Song, X. Bao, L. Liu, From water reduction to oxidation: Janus Co-Ni-P nanowires as high-efficiency and ultrastable electrocatalysts for over 3000 h water splitting, J. Power Sources, 330 (2016) 156-166.
[23] Q. Jing, Z. Wei, X. Ruijuan, L. Kaiqiang, W. Hong‐Yan, C. Mingxing, H. Yongzhen, C. Rui, Porous Nickel–Iron Oxide as a Highly Efficient Electrocatalyst for Oxygen Evolution Reaction, Adv. Sci., 2 (2015) 1500199.
[24] H. Liang, A.N. Gandi, D.H. Anjum, X. Wang, U. Schwingenschlögl, H.N. Alshareef, Plasma-Assisted Synthesis of NiCoP for Efficient Overall Water Splitting, Nano Lett., 16 (2016) 7718-7725.
[25] V.R. Jothi, R. Bose, H. Rajan, C. Jung, S.C. Yi, Harvesting Electronic Waste for the Development of Highly Efficient Eco-Design Electrodes for Electrocatalytic Water Splitting, Adv. Energy Mater., 8 (2018) 1802615.
[26] Y. Pan, K. Sun, S. Liu, X. Cao, K. Wu, W.-C. Cheong, Z. Chen, Y. Wang, Y. Li, Y. Liu, D. Wang, Q. Peng, C. Chen, Y. Li, Core–Shell ZIF-8@ZIF-67-Derived CoP Nanoparticle-Embedded N-Doped Carbon Nanotube Hollow Polyhedron for Efficient Overall Water Splitting, J. Am. Chem. Soc., 140 (2018) 2610-2618.
[27] Y. Zhang, Q. Shao, S. Long, X. Huang, Cobalt-molybdenum nanosheet arrays as highly efficient and stable earth-abundant electrocatalysts for overall water splitting, Nano Energy, 45 (2018) 448-455.
[28] H. Zhang, X. Li, A. Hähnel, V. Naumann, C. Lin, S. Azimi, S.L. Schweizer, A.W. Maijenburg, R.B. Wehrspohn, Bifunctional Heterostructure Assembly of NiFe LDH Nanosheets on NiCoP Nanowires for Highly Efficient and Stable Overall Water Splitting, Adv. Funct. Mater., 28 (2018) 1706847.
[29] Y. Zhou, Z. Wang, Z. Pan, L. Liu, J. Xi, X. Luo, Y. Shen, Exceptional Performance of Hierarchical Ni–Fe (hydr)oxide@NiCu Electrocatalysts for Water Splitting, Adv. Mater., 31 (2019) 1806769.
[30] D. Das, K.K. Nanda, One-step, integrated fabrication of Co2P nanoparticles encapsulated N, P dual-doped CNTs for highly advanced total water splitting, Nano Energy, 30 (2016) 303-311.
[31] S. Shit, S. Chhetri, W. Jang, N.C. Murmu, H. Koo, P. Samanta, T. Kuila, Cobalt Sulfide/Nickel Sulfide Heterostructure Directly Grown on Nickel Foam: An Efficient and Durable Electrocatalyst for Overall Water Splitting Application, ACS Appl. Mater. Interfaces, 10 (2018) 27712-27722.

[32] Y. Wu, X. Tao, Y. Qing, H. Xu, F. Yang, S. Luo, C. Tian, M. Liu, X. Lu, Cr-Doped FeNi–P Nanoparticles Encapsulated into N-Doped Carbon Nanotube as a Robust Bifunctional Catalyst for Efficient Overall Water Splitting, Adv. Mater., 31 (2019) 1900178.
[33] Z. Li, W. Niu, L. Zhou, Y. Yang, Phosphorus and Aluminum Codoped Porous NiO Nanosheets as Highly Efficient Electrocatalysts for Overall Water Splitting, ACS Energy Lett., 3 (2018) 892-898.
[34] M. Song, Y. He, M. Zhang, X. Zheng, Y. Wang, J. Zhang, X. Han, C. Zhong, W. Hu, Y. Deng, Controllable synthesis of Co2P nanorods as high-efficiency bifunctional electrocatalyst for overall water splitting, J. Power Sources, 402 (2018) 345-352.
[35] W. Li, X. Gao, D. Xiong, F. Xia, J. Liu, W.G. Song, J. Xu, S.M. Thalluri, M.F. Cerqueira, X. Fu, L. Liu, Vapor-solid synthesis of monolithic single-crystalline CoP nanowire electrodes for efficient and robust water electrolysis, Chem Sci, 8 (2017) 2952-2958.